Available online at www.sciencedirect.com

SCIENCE DIRECT®

Lithos 86 (2006) 229–244

LITHOS

www.elsevier.com/locate/lithos

The distribution of radiogenic heat production as a function of depth in the Sierra Nevada Batholith, California

Robert J. Brady [a,*], Mihai N. Ducea [b], Steven B. Kidder [b], Jason B. Saleeby [c]

[a] *Department of Geology and Geophysics, University of Calgary, 2500 University Dr. N.W., Calgary, Alberta, Canada T2N 1N4*
[b] *Department of Geological Sciences, University of Arizona, Tucson, AZ 85721, USA*
[c] *Division of Geological and Planetary Sciences, California Institute of Technology, M.S. 100-23, Pasadena, CA 9112, USA*

Received 26 July 2004; accepted 10 June 2005
Available online 27 July 2005

Abstract

Geochemical analyses and geobarometric determinations have been combined to create a depth vs. radiogenic heat production database for the Sierra Nevada batholith, California. This database shows that mean heat production values first increase, then decrease, with increasing depth. Heat production is ~2 $\mu W/m^3$ within the ~3-km-thick volcanic pile at the top of the batholith, below which it increases to an average value of ~3.5 $\mu W/m^3$ at ~5.5 km depth, then decreases to ~0.5–1 $\mu W/m^3$ at ~15 km depth and remains at these values through the entire crust below 15 km. Below the crust, from depths of ~40–125 km, the batholith's root and mantle wedge that coevolved beneath the batholith appears to have an average radiogenic heat production rate of ~0.14 $\mu W/m^3$. This is higher than the rates from most published xenolith studies, but reasonable given the presence of crustal components in the arc root assemblages. The pattern of radiogenic heat production interpreted from the depth vs. heat production database is not consistent with the downward-decreasing exponential distribution predicted from modeling of surface heat flow data. The interpreted distribution predicts a reasonable range of geothermal gradients and shows that essentially all of the present day surface heat flow from the Sierra Nevada could be generated within the ~35 km thick crust. This requires a very low heat flux from the mantle, which is consistent with a model of cessation of Sierran magmatism during Laramide flat-slab subduction, followed by conductive cooling of the upper mantle for ~70 m.y. The heat production variation with depth is principally due to large variations in uranium and thorium concentration; potassium is less variable in concentration within the Sierran crust, and produces relatively little of the heat in high heat production rocks. Because silica content is relatively constant through the upper ~30 km of the Sierran batholith, while U, Th, and K concentrations are highly variable, radiogenic heat production does not vary directly with silica content.

Keywords: Heat production; Heat flow; Sierra Nevada; Heat producing elements; Geothermal gradient

* Corresponding author. Tel.: +1 403 210 8691; fax: +1 403 284 0074.
E-mail address: rbrady@ucalgary.ca (R.J. Brady).

0024-4937/$ - see front matter © 2005 Elsevier B.V. All rights reserved.
doi:10.1016/j.lithos.2005.06.003

1. Introduction

Knowledge of the distribution of radiogenic heat production as a function of depth in the Earth is critical for the determination of crustal thermal and rheological structure, and provides an important constraint on geochemical, petrological, and tectonic models of crustal evolution (e.g., Turcotte and Oxburgh, 1972; Albarede, 1975; Buntebarth, 1976; Gosnold, 1987; Shapiro et al., 1999; Beaumont et al., 2001). However, variation of heat production with depth has rarely been empirically constrained (Lambert and Heier, 1967; Swanberg, 1972; Nicolaysen et al., 1981; Hart et al., 1981; Kremenetsky et al., 1989; Ketcham, 1996; Kumar and Reddy, 2004). Instead, heat production is typically assumed to decrease exponentially with depth, and the exponential is scaled to be consistent with surface heat flow data. The exponential distribution model for radiogenic heat production has seen widespread use and acceptance since it was first proposed by Lachenbruch (1968), but represents, at best, a gross simplification of the actual heat production profile in any particular geologic setting (c.f. Kremenetsky et al., 1989; Ketcham, 1996).

The exponential distribution model is based on the observation that co-located heat flow and near-surface heat production determinations within a particular heat flow province commonly fall on or near a line defined by the equation:

$$Q_0 = Q_R + DA_0$$

where Q_0 is the surface heat flow, Q_R is the reduced heat flow value (the intercept of the best fit line at $A_0=0$), D is the slope of the best-fit line through the data, and A_0 is the near-surface radiogenic heat production. The value of D is interpreted to represent the depth scale of variation of heat production, and Q_R the background heat flux (generally assumed to be the mantle contribution to total heat flux). This linear relationship could be explained by a model in which radiogenic heat production is constant from surface to a depth D, and then decreases to a regionally uniform value such that integrated heat production below that point is Q_R (Birch et al., 1968; Roy et al., 1968). This may be reasonable in so far as sheet-like plutons of near-constant thickness apparently are found at or near the surface in some cases (e.g., Birch et al., 1968; Roy et al., 1968), but is probably not widely applicable because such a model requires a very fortuitous history of magma emplacement and erosion to create a layer of plutons with laterally variable heat production (A_0) but constant thickness (D) over a large area. Lachenbruch (1968) proposed an exponential distribution model

$$A(z) = A_0 e^{-z/D}$$

where heat production, A, varies as a function of depth, z. This relationship is arguably more realistic in so far as it would produce the linear relationship of A_0 vs. Q_0 in spite of spatially variable erosion.

Lachenbruch (1968, 1970) noted that the exponential relationship had not been independently confirmed by depth vs. heat production studies, and his discussion infers that the model may apply only to a systematically differentiated granitoid crust.

While an exponential decrease of heat producing elements with depth provides an elegant mathematical alternative to the generation of empirical depth vs. heat production profiles, the model is not validated by direct measurements of the distribution of radiogenic heat production in the crust. Radiogenic heat production often changes in a discontinuous or stepwise pattern as lithology changes downward. In studies where upper crustal lithologies are included, heat production tends to first increase with depth, then decrease with depth (Hart et al., 1981; Nicolaysen et al., 1981; Ashwal et al., 1987; Kremenetsky et al., 1989; Ketcham, 1996). In cases where radiogenic heat production is seen to decrease downward, errors in heat production and/or depth determinations have been too large to test the exponential model (e.g., Swanberg, 1972; Swanberg and Blackwell, 1973; Nicolaysen et al., 1981). One study of depth vs. heat production within a single pluton from the Sierra Nevada, California was permissive of either a linear or an exponential depth distribution of heat production, but with a depth scale (D) of only 2.2 km (Sawka and Chapell, 1988), which is inconsistent with $D=10.1$ km for the Sierra Nevada as a whole (Lachenbruch, 1968). In addition to a lack of empirical evidence for an exponential depth distribution of heat producing elements (HPEs), modeling of realistic crustal structures has shown that it is possible to generate a linear heat production vs. heat flow relationship from a crust that has generally downward-

decreasing, but laterally highly variable, HPE abundance (e.g., Fountain et al., 1987).

If the exponential distribution model is correct anywhere, it is perhaps within large continental arcs or batholiths, where numerous magmatic bodies have long histories of melting, differentiation, and migration that could conceivably produce a systematic upward increase in incompatible HPE abundance. For example, data from the Closepet Batholith in the Dharwar Craton of southern India does show a roughly exponential distribution of radiogenic heat production over a paleodepth range of ~8–20 km (Kumar and Reddy, 2004). However, even in the end-member case of a crustal section that has undergone progressive fractionation upwards, there is no a priori reason for the heat producing element concentrations to decrease exponentially with depth.

Given the overall inability of the exponential distribution model for radiogenic heat production to accurately represent the results of most published empirical studies, it would be preferable to replace it with a set of empirically constrained models that define the probable patterns of crustal heat production, ideally one for each heat flow province (or at least one for each type and age of crust). This has previously been untenable, simply due to the great effort involved in acquiring a sufficient number of heat production measurements, and the lack of deep drill-holes or exhumed crustal sections with sufficient paleodepth control. However, modern mass spectrometry, combined with an increased number of well-understood tectonically exposed crustal sections, and an increased selection of reliable geobarometers, makes such efforts more feasible.

In this study, we compiled published U, Th and K concentration and geobarometry data on rocks from the California arc (Sierra Nevada and related terranes in California) in order to determine the heat production profile of the arc crust. We added 25 new heat production analyses from the southern Sierra Nevada and estimated the distribution of radiogenic heat production as a function of depth in the Mesozoic arc. We show that: (1) heat production generally decreases with depth, but not exponentially, (2) the heat producing elements are most abundant at paleo-depths of ~5 km where hydrothermal alteration is most pronounced, and limited amounts of fluid-saturated re-melting of granitoids and silicic volcanics may have occurred, and (3) the thickness of the felsic batholith ($\geq$30 km in California) is significantly greater than predicted from modeling of heat flow data.

2. Geology of the Sierra Nevada

The Sierra Nevada Batholith is an overall northward-plunging exposure of the upper ~35–42 km thick felsic-intermediate crust of the Jurassic to Cretaceous continental arc (Ague and Brimhall, 1988; Saleeby, 1990; Pickett and Saleeby, 1993; Fliedner et al., 1996); Fig. 1). Rocks exposed in the northern and central Sierra Nevada crystallized at depths of <4 km (~0.1 GPa; Ague, 1997) and include eruptive equivalents of the underlying intrusive rocks (Fiske and Tobisch, 1994), while those from the southernmost Sierra Nevada crystallized at ~25–30 km (0.7–0.9 GPa; Pickett, 1991; Pickett and Saleeby, 1993; Ague, 1997; Fig. 2). Low seismic velocities in the Sierran crust (~6.25 km/s; Savage et al., 1994; Ruppert et al., 1998; Fliedner et al., 2000; Ducea, 2001) support the assumption that exhumed felsic to intermediate rocks in the southern Sierra Nevada batholith are representative of unexhumed arc rocks to the north. Xenolith populations from Miocene volcanics in the central Sierra Nevada are consistent with this interpretation as they include felsic arc-related rocks; these volcanics plumb the upper mantle, but no good barometric indicators have been found for the felsic samples so it is not clear what depth they came from (Ducea and Saleeby, 1996).

In addition to the main body of the Sierra Nevada Batholith, a tectonically offset block of Sierran rocks crops out in the Santa Lucia Mts. of coastal California (Fig. 1; Hall, 1991). The Sierran affinity rocks in the Santa Lucia Mts. include tonalites, diorites, gabbros and metasediments. These rocks were exhumed from depths of ~26–40 km (0.75–1.0 GPa; Kidder et al., 2003, 2004).

Deeper portions of the Sierran arc lithosphere are sampled by small volumes of mafic to intermediate volcanics that erupted through the Sierra Nevada and carried xenoliths from depths of ~25 to 125 km (Dodge et al., 1986, 1988; Mukhopadhyay, 1989; Mukhopadhyay and Manton, 1994; Ducea and Saleeby, 1996; Saleeby et al., 2003). These volcanics

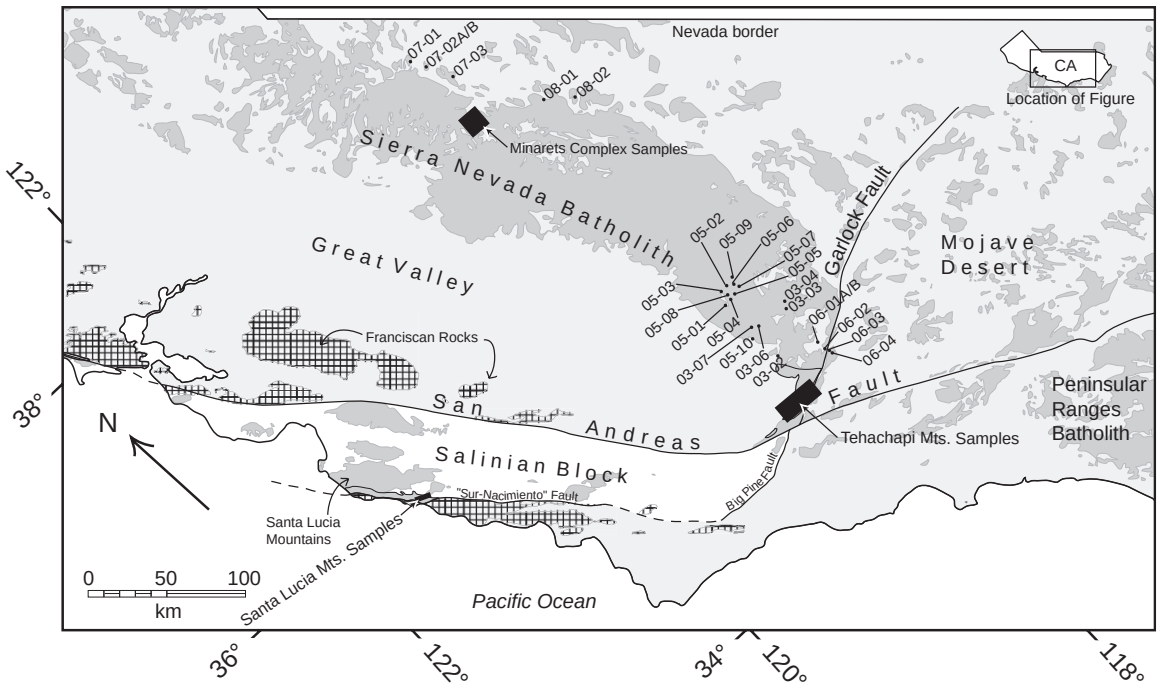

Fig. 1. Map showing numbered sample localities for new data points and general sample areas for previously published data within the main outcrop mass of the Sierra Nevada batholith and the tectonically offset equivalent in the Santa Lucia Mts.

occurred in two distinct intervals, one in the Mid-Miocene, and the other in the Plio–Pleistocene; each set shows a different sub-Sierran mantle lithosphere composition. The older volcanics include xenoliths that suggest the Sierra Nevada batholith was underlain by an eclogitic root (the garnet and pyroxene-rich

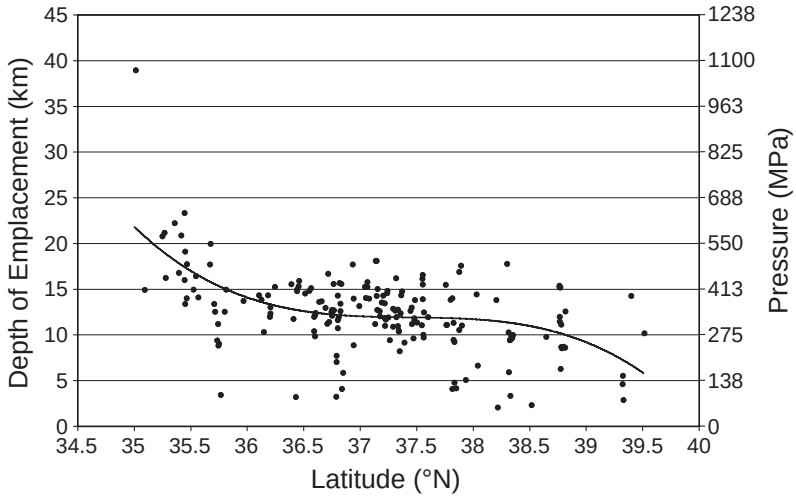

Fig. 2. Latitude versus depth of emplacement determined with aluminum-in-hornblende barometry for plutonic rocks of the Sierra Nevada batholith (3 new determinations plus data from: Ague and Brimhall, 1988; Ague, 1997; Ague, pers. comm.). Note that the data reflect an overall northward plunge of the batholith, with the southern ~100 km plunging most steeply (trendline is a best fit 3rd order polynomial). The significant scatter of data at any given latitude is largely due to east–west variations in exhumation across the ~120-km-wide batholith.

residue of the batholith) from ~40 to 75 km, and mantle wedge peridotites to ~125 km (Ducea and Saleeby, 1996, 1998c). In contrast, the younger volcanics include no eclogitic material; instead mantle peridotites begin immediately beneath the felsic crust, from depths of ~40 km downward. This change in composition has been interpreted as being caused by foundering of the batholith root, and replacement by upper mantle material (Ducea and Saleeby, 1998a; Saleeby et al., 2003). Because we are interested in constructing a depth vs. heat production profile for the Jurassic–Cretaceous crust; we will only consider data from the older xenolith sample suite.

3. Samples and techniques

The depth vs. heat production model was constructed using geobarometric and U, Th, and K concentration data from 82 sample locations within the California arc. For 57 of these locations, data were obtained from published geochemical, geobarometric, and stratigraphic studies (Dodge et al., 1986; Pickett and Saleeby, 1993; Holt, 1994; Lowe, 1995; Ducea and Saleeby, 1998c; Ducea et al., 2003; Kidder et al., 2003). The largest remaining data gaps, as a function of depth, were filled with new analytical data from 25 locations.

For most locations, paleo-depth determinations and corresponding geochemical measurements were made on samples collected from the same outcrop. However, for two samples from the Sierra Nevada Mts., as well as the samples from the Tehachapi and Santa Lucia Mts., geobarometric and geochemical determinations were not co-located; rather, paleo-depth values were calculated by linear interpolation between nearby geobarometric determinations. In all cases paleo-depths represent Late Cretaceous sample depths, as all sampled lithologies were emplaced or deposited during that time interval (Ducea, 2001).

For the newly analyzed samples, HPE abundances were determined by measuring concentrations of ^{39}K, ^{238}U, and ^{232}Th in dissolved samples of whole rock using quadrupole Inductively Coupled Plasma Mass Spectrometry (ICPMS) at the University of Victoria and California State University, Bakersfield. This involved crushing and powdering of >300 g of rock down to a grain size of <60 μm, followed by multi-step dissolution of 50 to 100 mg aliquots in hot, concentrated nitric, hydrofluoric, and boric acids. Analytical precision for these elements with the ICPMS

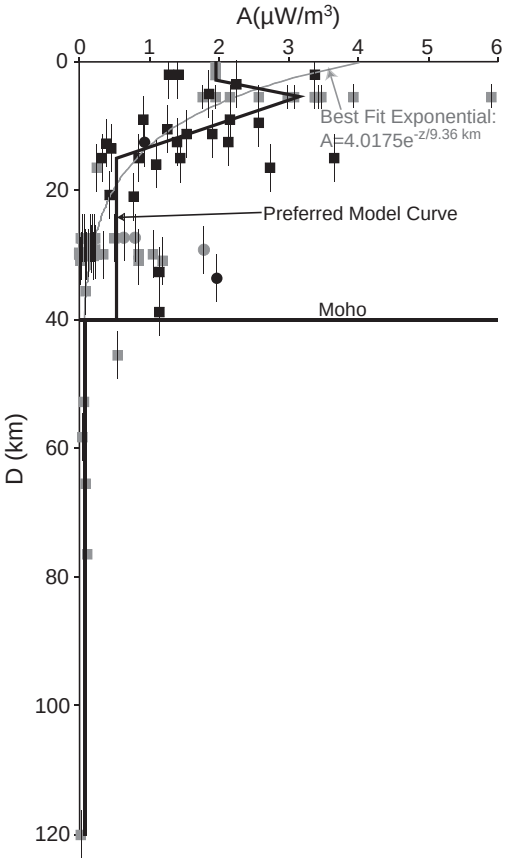

Fig. 3. Paleodepth vs. radiogenic heat production plot for the Sierra Nevada batholith. Data from published literature shown in grey (see Table 1 for details), new data shown in black. Circles represent metasediments, all data from igneous and meta-igneous rocks shown as squares. Depth error bars represent average ± 1 kb errors for a variety of barometric determinations, except for the samples from the Minarets Caldera complex. The bar from 0 to 3 km depth represents 61 samples from the Minarets Caldera ignimbrite, and is plotted over a depth range equal to the measured stratigraphic thickness of the ignimbrite (Fiske and Tobisch, 1994; Holt, 1994; Lowe, 1995). Samples plotted at 5.5 km depth come from a variety of plutons in the Minarets and Merced Peak area and are plotted at this depth because in situ melts fall between the PH_2O=1 kb and PH_2O=2kb cotectics of the quartz+albite+orthoclase system (Lowe, 1995; Tuttle and Bowen, 1958). The error bars on heat productivity determinations are smaller than the symbols. Moho depth is plotted at 40 km, consistent with the crustal structure suggested by xenolith studies (Ducea and Saleeby, 1996, 1998a) and geophysical data (Fliedner et al., 1996; Wernicke et al., 1996).

Table 1
Radiogenic element abundances and depth control data for samples of the Sierra Nevada batholith

Sample #	Lithology[a,b]	^{39}K (%)	^{238}U (ppm)	^{232}Th (ppm)	A_0 (K) (μW/m^3)	A_0 (U) (μW/m^3)	A_0 (Th) (μW/m^3)	A_0 (Total) (μW/m^3)	P (GPa)	D[c] (km)	Source[d]
06-02	I	2.65	1.06	8.75	0.25	0.28	0.62	1.15	0.9	32.7	1
06-04	I	3.30	0.74	9.04	0.31	0.19	0.64	1.15	1.07	38.9	2
05-07	I	3.40	3.69	12.23	0.32	0.97	0.87	2.16	0.24	8.8	3
05-02	I	1.41	2.19	9.68	0.13	0.57	0.69	1.39	0.34	12.5	3
06-03	M	4.05	3.52	9.51	0.38	0.92	0.67	1.98	0.93	33.7	1
05-09	I	2.67	5.18	28.79	0.25	1.36	2.04	3.65	0.41	15.0	3
07-02A	I	3.10	2.30	7.30	0.29	0.60	0.52	1.41	0.06	2.0	3
08-02	I	4.83	1.71	5.03	0.46	0.45	0.36	1.26	0.29	10.4	3
05-06	I	3.37	3.37	14.61	0.32	0.88	1.04	2.24	0.10	3.5	3
08-01	I	2.82	4.86	5.24	0.27	1.28	0.37	1.91	0.31	11.2	3
07-02B	I	1.85	1.98	8.47	0.17	0.52	0.60	1.29	0.06	2.0	3
07-03	I	3.98	4.42	4.48	0.38	1.16	0.32	1.85	0.14	5.1	3
06-01A	I	1.53	2.05	2.38	0.14	0.54	0.17	0.85	0.41	14.9	2
06-01B	I	1.99	1.20	13.28	0.19	0.31	0.94	1.44	0.41	14.9	2
05-10	I	1.33	0.79	1.91	0.13	0.21	0.14	0.47	0.37	13.4	3
05-03	M	3.73	1.62	2.23	0.35	0.43	0.16	0.94	0.34	12.5	3
03-04	I	2.30	1.28	7.76	0.22	0.34	0.55	1.10	0.44	16.0	2
05-05	I	3.14	2.85	21.64	0.30	0.75	1.53	2.58	0.26	9.4	3
05-01	I	3.20	4.35	9.77	0.30	1.14	0.69	2.14	0.34	12.5	3
05-08	I	2.00	1.41	4.97	0.19	0.37	0.35	0.91	0.24	8.8	3
03-02	I	1.40	0.63	1.83	0.13	0.17	0.13	0.43	0.57	20.8	3
03-03	I	0.90	1.23	5.27	0.08	0.32	0.37	0.78	0.57	20.9	3
07-01	I	3.30	5.82	21.65	0.31	1.53	1.53	3.37	0.06	2.1	3
05-04	I	2.90	2.52	8.64	0.27	0.66	0.61	1.55	0.31	11.2	3
03-07	I	0.50	0.87	0.50	0.05	0.23	0.04	0.31	0.41	15.0	3
03-06	I	2.60	4.46	18.41	0.25	1.17	1.30	2.72	0.45	16.5	3
709.2	I	1.30	1.00	1.60	0.12	0.26	0.11	0.50	0.75	27.3	4
730.3	I	0.70	0.00	0.00	0.07	0.00	0.00	0.07	0.75	27.3	4
802.6	I	0.92	0.00	0.60	0.09	0.00	0.04	0.13	0.75	27.3	4
813.2	I	1.14	0.00	1.10	0.11	0.00	0.08	0.19	0.75	27.3	4
813.1	I	1.80	0.00	0.60	0.17	0.00	0.04	0.21	0.75	27.3	4
814.2	I	0.43	0.00	0.60	0.04	0.00	0.04	0.08	0.75	27.3	4
814.9	I	0.37	0.00	0.00	0.03	0.00	0.00	0.03	0.75	27.3	4
817.1	I	0.76	0.00	0.00	0.07	0.00	0.00	0.07	0.75	27.3	4
812.1	I	0.36	0.00	0.00	0.03	0.00	0.00	0.03	0.75	27.3	4
814.12	I	0.41	0.00	0.00	0.04	0.00	0.00	0.04	0.75	27.3	4
718.3	I	0.88	0.00	2.00	0.08	0.00	0.14	0.22	0.75	27.3	4
711.3	M	0.24	0.80	8.20	0.02	0.21	0.58	0.81	0.75	27.3	4
815.3B	M	2.42	0.00	6.00	0.23	0.00	0.43	0.65	0.75	27.3	4
TC-8	M	3.07	3.20	9.90	0.29	0.84	0.70	1.79	0.80	29.1	5
CM-9	I	1.54	0.29	0.63	0.15	0.08	0.04	0.26	0.45	16.4	5
GC-17	I	0.94	0.14	0.00	0.09	0.04	0.00	0.12	0.83	30.2	5
PC175	I	0.04	0.02	0.00	0.00	0.01	0.00	0.01	0.82	29.8	5
PTC42	I	1.12	0.80	0.52	0.11	0.21	0.04	0.35	0.82	29.8	5
TC-9	I	0.14	0.02	0.00	0.01	0.00	0.00	0.02	0.85	30.9	5
TC-19	I	0.09	0.02	0.00	0.01	0.01	0.00	0.01	0.85	30.9	5
TC42	I	1.07	0.14	0.00	0.10	0.04	0.00	0.14	0.82	29.7	5
TC45b	I	0.75	0.11	0.00	0.07	0.03	0.00	0.10	0.82	29.7	5
TC-47	I	0.04	0.02	0.00	0.00	0.00	0.00	0.01	0.82	29.7	5
TC49b	I	0.16	0.02	0.08	0.02	0.01	0.01	0.03	0.83	30.2	5
TC-83	I	0.18	0.02	0.00	0.02	0.01	0.00	0.02	0.85	30.9	5
GC-1	I	1.25	0.22	3.00	0.12	0.06	0.21	0.38	0.35	12.7	5
GC-14	I	0.75	0.12	11.00	0.07	0.03	0.78	0.86	0.85	30.9	5

Table 1 (*continued*)

Sample #	Lithology[a,b]	^{39}K (%)	^{238}U (ppm)	^{232}Th (ppm)	A_0 (K) (μW/m^3)	A_0 (U) (μW/m^3)	A_0 (Th) (μW/m^3)	A_0 (Total) (μW/m^3)	P (GPa)	D[c] (km)	Source[d]
GC-23	I	0.97	0.16	0.00	0.09	0.04	0.00	0.13	0.83	30.2	5
GC-33	I	1.44	0.23	0.07	0.14	0.06	0.00	0.20	0.83	30.2	5
GC-43	I	2.78	0.30	7.50	0.26	0.08	0.53	0.86	0.82	29.8	5
GC-50	I	1.36	0.19	0.00	0.13	0.05	0.00	0.18	0.80	29.1	5
GC-55	I	1.11	0.20	1.30	0.10	0.05	0.09	0.25	0.82	29.8	5
GC-60	I	0.36	0.03	0.00	0.03	0.01	0.00	0.04	0.82	29.8	5
PC35P	I	4.16	1.00	5.90	0.39	0.26	0.42	1.05	0.82	29.8	5
TC-6	I	3.12	0.25	12.00	0.29	0.07	0.85	1.18	0.85	30.9	5
TC12b	I	1.07	0.17	0.00	0.10	0.04	0.00	0.14	0.78	28.4	5
TC-34	I	1.16	0.50	0.00	0.11	0.13	0.00	0.24	0.80	29.1	5
Bc218	E	0.25	0.05	0.00	0.03	0.02	0.00	0.05	1.60	58.2	6
B75	G	0.17	0.18	0.19	0.02	0.06	0.02	0.09	0.98	35.7	6
F34	E	0.11	0.03	0.02	0.01	0.01	0.00	0.02	3.30	120.1	6
Bc207	E	0.29	0.12	0.19	0.03	0.04	0.02	0.09	1.80	65.5	6
G39	G	0.24	0.22	0.11	0.03	0.07	0.01	0.11	2.10	76.4	6
G36	E	0.19	0.10	0.07	0.02	0.03	0.01	0.06	1.45	52.8	6
MCI[e]	V	3.46	3.93	13.21	0.28	0.88	0.80	1.96		1.5	7
PPLP[f]	I	3.71	4.00	22.50	0.35	1.05	1.59	2.99	0.15	5.5	8
RPLP[g]	I	3.78	2.50	16.00	0.36	0.66	1.13	2.15	0.15	5.5	8
PPL[h]	I	4.12	4.00	23.00	0.39	1.05	1.63	3.07	0.15	5.5	8
RPL[i]	I	3.82	5.50	22.00	0.36	1.44	1.56	3.36	0.15	5.5	8
NCL[j]	I	4.29	9.00	44.33	0.40	2.36	3.14	5.91	0.15	5.5	8
SLG[k]	I	4.11	5.39	23.56	0.39	1.41	1.67	3.47	0.15	5.5	8
MPM[l]	V	3.10	4.27	16.33	0.29	1.12	1.16	2.57	0.15	5.5	8
JLG[m]	I	2.67	3.55	10.91	0.25	0.93	0.77	1.96	0.15	5.5	8
TKL[n]	I	3.72	6.50	19.17	0.35	1.71	1.36	3.42	0.15	5.5	8
PPME[o]	I	2.10	3.67	8.67	0.20	0.96	0.61	1.78	0.15	5.5	8
RMV[p]	I	4.43	6.78	24.44	0.42	1.78	1.73	3.93	0.15	5.5	8
CP71	P	0.80	1.40	0.20	0.09	0.45	0.02	0.56	1.25	45.5	9

Note: Radiogenic heat production is calculated by assuming total K=99.9881% ^{39}K+0.119% ^{40}K, total U=99.28% ^{238}U+0.72% ^{235}U, total Th=100% ^{232}Th and elemental heat production=0.0035 μW/kg for Th, 96.7 μW/kg for U, and 26.3 μW/kg for Th (Emsley, 1989; Jessop, 1990).

[a] E=eclogite, G=granulite, I=intrusive igneous, M=metasediment, P=peridotite, V=volcanic.

[b] Densities were not measured for each sample, instead reasonable average values were assigned for each lithology. Assigned densities for each lithology were: E,P,G=3300 kg/m^3 ; I,M=2695 kg/m^3 ; V=2695 kg/m^3 or 2300 kg/m^3 for the Minarets Caldera Ignimbrite.

[c] All pressure to depth conversions assume a constant density of 2695 kg/m3 (3.64 km/kbar).

[d] 1=geobarometric value interpolated from data in Pickett and Saleeby (1993) and Ague and Brimhall (1988); 2=geobarometric value newly acquired Al-in-hornblende; 3=geobarometric value from Ague and Brimhall (1988); 4=geobarometric value and geochemical data from Kidder et al. (2003); 5=geobarometric value and geochemical data from Pickett (1991); 6=geobarometric value from Ducea and Saleeby (1998c); 7=samples collected through the entire ~3 km thickness of the Minarets Caldera Ignimbrite (Holt, 1994), all data assigned to a median depth of 1.5 km. Geochemical data from Lowe (1995); 8=geobarometric value interpreted from melt composition and pluton emplacement at base of Minarets volcanic pile (Tuttle and Bowen, 1958; Lowe, 1995) Geochemical data from Lowe (1995); 9=geobarometric value and geochemical data from Dodge et al. (1986).

[e] Geochemical values represent the average of 61 samples of Minarets Complex Ignimbrite.

[f] Geochemical values represent the average of 2 samples of Post Peak Leucogranite Porphyry.

[g] Geochemical values represent the average of 2 samples of Red Peak Leucogranite Porphyry.

[h] Geochemical values represent the average of 4 samples of Post Peak Leucogranite.

[i] Geochemical values represent the average of 2 samples of Red Peak Leucogranite.

[j] Geochemical values represent the average of 3 samples of Norris Creek Leucogranite.

[k] Geochemical values represent the average of 18 samples of Shellenbarger Lake Granites.

[l] Geochemical values represent the average of 33 samples of Merced Peak Metavolcanics.

[m] Geochemical values represent the average of 11 samples of Jackass Lakes Granodiorite.

[n] Geochemical values represent the average of 6 samples of Timber Knob Leucogranite.

[o] Geochemical values represent the average of 3 samples of the Post Peak mafic enclave.

[p] Geochemical values represent the average of 9 samples of re-melted Merced Peak Metavolcanics.

method ranges from ± 3% (U and Th) at 2σ to ± 10% at 2σ (K). In order to monitor accuracy of the procedure, aliquots of USGS standard whole rock powder GSP-1 were dissolved and analyzed concurrently with the unknown samples; measured values overlapped with accepted standard values within 2σ analytical errors.

For 22 of the newly analyzed samples, no new geobarometric determinations were necessary, as 21 of the samples were collected from the same outcrops as those used by Ague and Brimhall (1988; exact locations and barometric determinations provided by Ague, pers. comm.), and one of them was collected within a few km's of samples previously analyzed by Ague and Brimhall (1988) and Pickett and Saleeby (1993). New geobarometric determinations were made for three of the samples using the Aluminum-in-hornblende barometer (Hammarstrom and Zen, 1986); all aluminum-in-hornblende barometric determinations, including those from Ague and Brimhall (1988) were re-calculated using the calibration of Schmidt (1992).

Radiogenic heat production was calculated for each rock sample using accepted values of elemental heat generation (Emsley, 1989; Jessop, 1990), with the assumption that all isotopes of each element occurred in natural abundances. A reasonable average density was assigned for each major rock type (granitoids and high grade metamorphic rocks: 2695 kg/m^3, ignimbrites: 2300 kg/m^3, eclogites, granulites, and peridotites: 3300 kg/m^3).

4. Results

Depth of emplacement, HPE abundances, and radiogenic heat production values for the 82 sample sites are reported in Fig. 3 and Table 1. In most cases, HPE abundance data reported for each site represent the results from a single sample, collected from an intact outcrop of essentially uniform lithology. In the case of data reported for sample sites from the Minarets region of the Sierra Nevada, the results for each sample site represent an average of all analyses of numerous hand samples (from 2 to 61) collected from a single geologic unit; samples may have been collected as far as 2.5 km apart within each unit (Lowe, 1995).

The resulting depth vs. heat production plot shows a definite depth-dependent pattern, in spite of significant scattering of heat production values at any given depth (Fig. 3). The upper 3 km of the sampled Sierran Crust, comprising the Minarets Complex ignimbrites, has an average heat production value of 1.96 μW/m^3. Heat production increases below this point, with the highest values occurring between approximately 5 and 10 km paleodepth, where measured heat production has a median value of 3.41 μW/m^3, and a peak value of 5.91 μW/m^3. Between 10 and 40 km paleodepth the median heat production value is 1.82 μW/m^3. Below 40 km paleodepth, radiogenic heat production decreases drastically, having an average value of 0.14 μw/m^3 between ~40 and 125 km.

5. Discussion

Our empirically constrained depth vs. heat production plot for the Sierra Nevada batholith is the first direct test of the exponential distribution model proposed by Lachenbruch (1968) for this batholith, and shows significant deviations from the predictions of that model. While the observed overall downward decrease in radiogenic heat production is suggestive of an exponential curve, a calculated best-fit exponential fails to predict most of the highly radiogenic material in the 5 to 10 km depth range, and falls far below the median values for radiogenic heat production below 20 km depth (Fig. 3).

As an alternative to an exponential curve, an interpretive, empirically constrained model curve was constructed (Fig. 3). Because this curve is based on data from Late Cretaceous xenoliths, intrusions, and metamorphic screens, it represents a Late Cretaceous depth vs. heat production profile for the Sierra Nevada batholith. This depth vs. heat production profile may be a valid representation of heat production in the Sierran crust and upper mantle from Late Cretaceous until Late Miocene time, because there was apparently no major alteration of the Sierran crust and uppermost mantle until delamination of the Sierran root occurred some time after ~8–12 Ma (Ducea and Saleeby, 1998a). The middle and upper crustal portions of this curve should still apply to the central and northern Sierra Nevada, if the batholith is more-or-less intact and northward-plunging (Ague and Brimhall, 1988; Saleeby, 1990; Pickett and Saleeby, 1993; Fliedner et al., 1996). However, the interpreted Miocene or younger delamination of the Sierran crustal root means that

the curve should not apply to the deeper portions of the modern Sierra Nevada batholith. Futhermore, tectonic unroofing of the southern Sierra Nevada (Saleeby, 2003) means that this profile is not expected to be representative of that region except at the surface.

The upper 3 km of the interpretive model curve is fixed by the measured heat production value (1.96 μW/m^3) of the Minarets Ignimbrite (Holt, 1994). Below that point, the curve increases linearly to the mean value for the shallow intrusives at the base of the Minarets Caldera Complex (3.15 μW/m^3 at 5.5 km). It then decreases linearly to a value of 0.53 μW/m^3 at 15 km depth, below which it remains constant to the base of the crust at 40 km. This constant value through the middle to lower crust seems reasonable not just as a mean value for the observed data, but also because the well-exposed Sierra Nevada batholith shows no significant average lithological/compositional changes through most of this depth range (Saleeby, 1990; Ducea, 2001, 2002; Saleeby et al., 2003). The slopes from 3–5.5 and 5.5–15 km depth are chosen to be linear for simplicity, and because there is insufficient control to justify a more complex curve shape.

Although the interpretive model curve is probably only a valid representation until Late Miocene time, its predictions regarding surface heat flow can be compared to modern surface heat flow measurements because the thermal effects of the interpreted Miocene or younger lower crustal delamination should require several tens of millions of years to be conductively transmitted through the crust (c.f. Dumitru, 1990). It predicts a value of crustal heat production that falls within the range of values calculated for average surface heat flow, implying a low mantle heat flux. It predicts 42.3 mW of crustal heat production beneath each square meter of the Sierran surface, while average surface heat flow in the Sierra Nevada is between 36 and 52 mW/m^2, depending on whether or not anomalously hot values are filtered out of the data set (Saltus and Lachenbruch, 1991). These values permit a maximum mantle heat flux of ~10 mW/m^2 at ~10 Ma.

The steady-state geotherm predicted by the interpretive model depends on the value that is chosen for heat flux from the mantle (Fig. 4). Although mantle heat flux is poorly constrained, both modeling of surface heat flow data (Saltus and Lachenbruch, 1991) and interpretation of our data set suggest that it is between 0 and 20 mW/m^2. Using this range of values, the predicted basal crustal temperatures range from ~330 to ~730 °C. The upper part of this range of values seems reasonable, as it overlaps with the deep crust–upper mantle equilibration temperatures of between ~570 and 750 °C, recorded geothermometri-

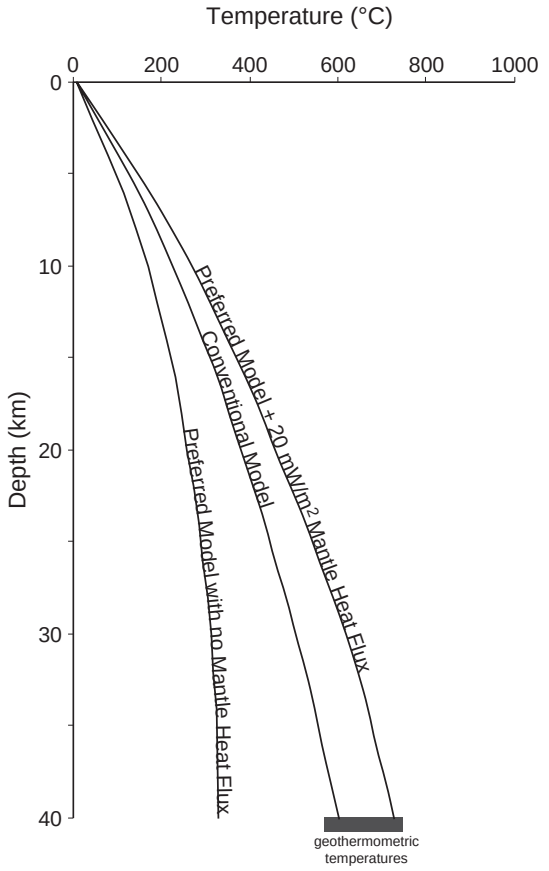

Fig. 4. Calculated steady-state crustal geotherms for the preferred interpretive model assuming two extreme values of heat flux from the mantle to illustrate the total reasonable range of predicted crustal temperatures (min. mantle flux: 0 mW/m^2; max. mantle flux: 20 mW/m^2; see text for discussion), and for the conventional exponential distribution model. In all cases, thermal conductivity remained between 1.95 and 2.2 Wm^{-1} K^{-1}, varying as a function of temperature (Cull, 1976), heat capacity was fixed at 800 Jkg^{-1} K^{-1}, crustal density was fixed at 2695 kg m^{-3}, and the coefficient of thermal expansion was fixed at 1×10^{-5} K^{-1}. For the conventional exponential model, the accepted average Sierran surface heat flow of 36 mW/m^2 was used, along with a D value of 10 km and Q_R of 17 mW/m^2 (Saltus and Lachenbruch, 1991); Q_R was assumed to represent the heat flux from the mantle. The grey box labeled "geothermometric temperatures" corresponds to the range of temperatures determined from Miocene lower crustal samples (Ducea and Saleeby, 1996; Lee et al., 2000).

cally in Miocene samples (Ducea and Saleeby, 1996; Lee et al., 2000).

If the geothermometrically derived deep crust–upper mantle temperature data are used to constrain the permissible basal crustal temperature, and crustal heat production is assumed to be represented by the interpretive model curve, then the heat flux from the mantle in Miocene time is limited to a range of 11 to 20 mW/m^2. The low end of this range is roughly coincident with ~10 mW/m^2 value suggested above by subtraction of the total model crustal heat production from the average observed surface heat flow.

The suggestion that nearly all of the surface heat flow comes from crustal radiogenic heat production, and mantle heat flux is very low, is also consistent with the results of modeling of fission track data, which suggests rapid cooling of the Sierran crust between ~75 and 65 Ma (Dumitru et al., 1991).

This rapid cooling of the Sierran crust was originally interpreted as occurring due to direct contact with a shallowly dipping oceanic slab that was subducted during the Laramide orogeny (Henyey and Lee, 1976; Dumitru et al., 1991), but xenolith evidence for an intact subbatholith mantle lithosphere into the Miocene (Ducea and Saleeby, 1996, 1998c) disallows the possibility of direct contact between the continental crust and subducting slab. An alternative model for Laramide cooling under the Sierra Nevada batholith has been proposed by Saleeby (2003), who suggests that asthenospheric corner flow between the Laramide slab and the Sierran batholith was cut off by shallowing of the subduction angle of an ~500-km-wide portion of the slab that extended NNE from southern California into southern Wyoming (i.e., immediately inboard of the Sierra Nevada batholith). This should result in a cessation of arc magmatism and conductive cooling of the sub-Sierran upper mantle since the latest Cretaceous or Early Paleogene, consistent with both the apatite fission track data and evidence from upper mantle xenoliths that suggests Phanerozoic cooling from $\geq$1100 to $\leq$800 °C (Lee et al., 2000; Saleeby et al., 2003).

The conductive cooling of mantle lithosphere under the Sierra Nevada apparently ceased in the Late Miocene or Pliocene, when the cold mantle lithosphere was replaced by hot mantle asthenosphere, but this change has not yet affected the surface heat flow. Plio–Pleistocene xenolith thermobarometry, petrography, and geophysical data all show the presence of high-temperature, partial-melt-bearing asthenosphere under much of the Sierra Nevada (Wernicke et al., 1996; Ducea and Saleeby, 1998a,b). This asthenosphere is thought to have been emplaced as a result of delamination of the cold, dense Sierran root, and is at least temporally related to Basin and Range extension (Ducea and Saleeby, 1998a; Zandt, 2003). The thermal pulse that should be generated by the emplacement of hot asthenosphere has not yet reached the surface; this is consistent with the $\geq$10 Ma that should be required for the crust to re-establish a nearly steady state conductive geotherm (c.f. Dumitru, 1990).

The depth vs. heat production plot (Fig. 3) clearly shows an interval of high radiogenic heat production from ~5–10 km depth, which might represent a zone of hydrothermal deposition of HPE-rich minerals or a zone of emplacement of highly differentiated HPE-rich granitoids (Fig. 5). Both hydrothermal alteration and magmatic differentiation have been proposed as primary controls on the distribution of HPEs in plutonic environments (e.g., Lachenbruch, 1970; Gosnold, 1987; Sawka and Chappell, 1988). Because our current data set was designed to provide a crustal-scale perspective on the distribution of radiogenic heat production, it does not include detailed information about the distribution of U, Th, and K within each sample, as would be necessary to confidently separate the effects of these two mechanisms. Further work, including detailed petrography and determination of the distribution of HPEs in primary and secondary minerals will be necessary to constrain the controls on HPE distribution in the Sierra Nevada batholith.

Although we do not have sufficient data to determine what process(es) control the distribution of HPEs in the Sierra Nevada batholith, we can demonstrate that there is no strong correlation between HPE abundance and silica content. Silica content in the upper 30 km of the Sierran crust is relatively invariant (average ~62% SiO_2); the average crust has the composition of a granodiorite at shallow levels (0–15 km) and closer to a tonalite at greater depths (15–30 km; Saleeby, 1990; Ducea, 2001; Ducea et al., 2003). In contrast, U and Th concentrations vary by a factor of ~5 with depth (K concentrations also vary, but to a lesser extent).

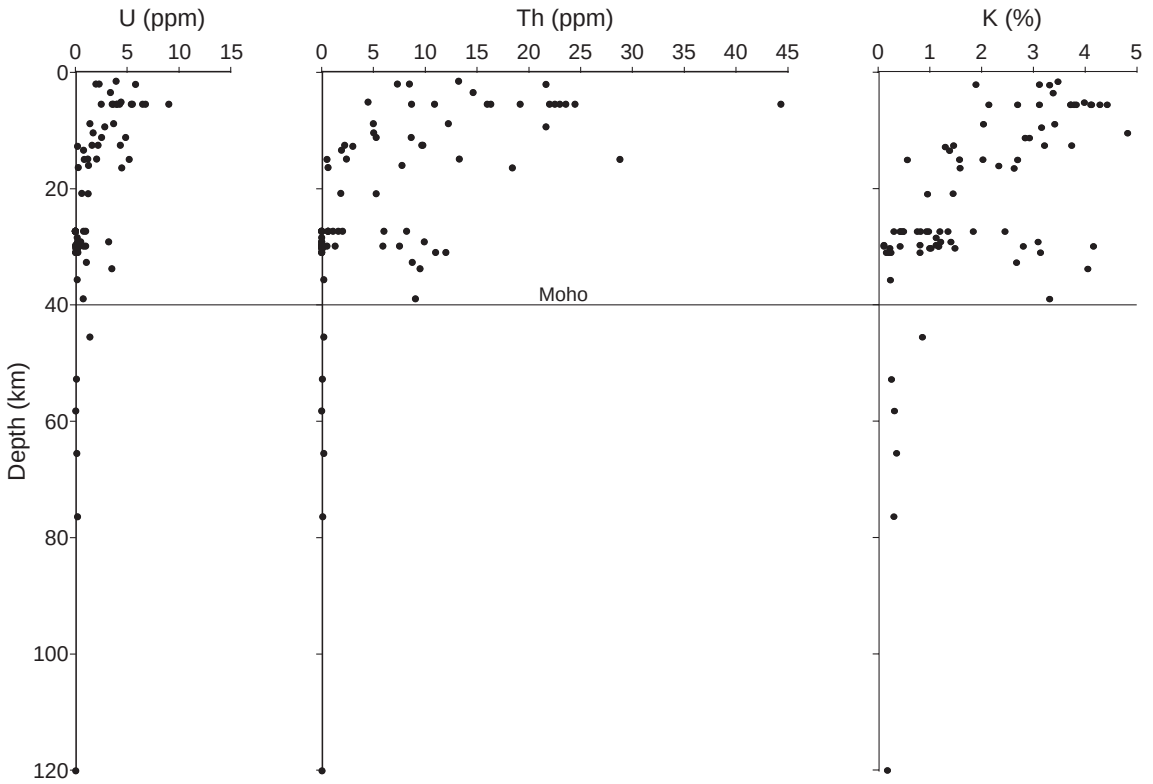

Fig. 5. Paleodepth vs. U, Th, and K concentration for the Sierra Nevada batholith. Note that U and Th values vary more than K values as a function of depth; comparison with Fig. 3 clearly shows that intervals of high radiogenic heat production are dominantly due to high U and/or Th concentrations. Errors on concentration values are smaller than the symbols; refer to Fig. 3 for depth determination errors.

The apparent lack of correspondence between silica content and radiogenic heat production in our data set from the Sierran crust implies that seismic velocities cannot reliably be used as a proxy for radiogenic heat production. This result is in general agreement with the conclusions of Fountain (1986), who used rock density and HPE measurements from the Archean Superior province of North America to suggest that heat production cannot be reliably predicted from seismic velocity. It is in disagreement with earlier studies, most noteably Rybach and Buntebarth (1984), who concluded that seismic P-wave velocities are exponentially related to rates of radiogenic heat production because both are related to the cation packing index of rocks.

Our interpretations regarding the use of seismic velocities to infer HPE abundance agree with and strengthen the conclusions drawn by Fountain (1986), but because our data set deals with a large number of polymineralic rock samples it arguably provides a more direct test of the model of Rybach and Buntebarth (1984). Rybach and Buntebarth (1987) suggested that the criticism of Fountain (1986) of their model was not valid because his sample set was " arbitrarily selected, probably atypical rock types," including anomalous rock types and possibly monomineralic rock types, while their seismic velocity–HPE abundance relationship was a stochastic one, valid for large sample sets of polymineralic rocks.

Our data set is relatively large ($n=225$) and is dominated by polymineralic intrusive rock types (Table 1), and it suggests that there is no simple correspondence between silica content and HPE abundance. Therefore, although silica content might reasonably be inferred from seismic velocities (Christensen and Mooney, 1995), HPE abundance probably cannot be. As pointed out by Fountain (1986), this is probably due

to the fact that seismic velocities are dominantly controlled by the abundant minerals in a rock (often quartz and feldspars), while HPE abundance (particularly U and Th) are dominantly controlled by the accessory minerals.

The lack of correspondence between silica content and HPE abundance in our data set also suggests that the modeled thickness of a radiogenic-rich layer in the crust is not necessarily representative of the thickness of a felsic intrusion or layer of intrusions.

In addition to constraining crustal heat production, the paleodepth vs. radiogenic heat production database provides valuable constraints on upper mantle heat production. Upper mantle heat production data are important in constraining mantle heat fluxes and models of lithospheric structure (e.g., Rudnick et al., 1998; Jaupart and Mareschal, 1999), but such data are very limited in number, and modeling of lithospheric thermal structure for any given heat flow province is therefore generally dependent on extrapolation of xenolith data from elsewhere.

In the case of the Sierra Nevada batholith, xenoliths suitable for both geobarometric and geochemical analyses are available, and they suggest that the upper mantle had a mean radiogenic heat production rate of 0.069 μW/m3 (Fig. 3; excluding the highly radiogenic sample at 45.5 km). In addition, several mantle xenoliths have been sampled that have no direct geobarometric control, but for which HPE analyses are available. If these xenoliths are added to the calculation, mean upper mantle heat production is ~0.14 μW/m^3 (n=23; Table 2). These values are higher than most other reported averages for upper mantle heat production (0.02–0.09 μW/m^3, excluding kimberlites; (Rudnick et al., 1998). Most of these estimates however come from Archean crustal sections, where ongoing radioactive decay through ~3 Ga means that heat production has decreased by a factor of ~2 since the Mid-Archean. Furthermore, the sub-Sierran mantle wedge xenolith suite shows evidence of slab-derived fluid enrichment in incompatible elements, including K, U, and

Table 2
Radiogenic element abundance data for Sierran xenoliths

Sample#	Lithology	Density[a]	K_2O %	^{39}K %	U (ppm)	Th (ppm)	A_0 (K) (μW/m^3)	A_0 (U) (μW/m^3)	A_0 (Th) (μW/m^3)	A_0 (Total) (μW/m^3)
BC216	Eclogite	3300	0.37	0.31	0.122	0.201	0.035	0.039	0.017	0.092
BC221	Gar–websterite	3300	0.25	0.21	0.108	0.212	0.024	0.034	0.018	0.077
BC218	Eclogite	3300	0.09	0.07	0.051	0.005	0.009	0.016	0.000	0.025
96F34	Gar–websterite	3300	0.13	0.11	0.036	0.017	0.012	0.011	0.001	0.025
BC207	Carbonate eclogite	3300	0.05	0.04	0.724	0.189	0.005	0.231	0.016	0.252
96G39	Eclogite	3300	0.22	0.18	0.221	0.113	0.021	0.070	0.010	0.101
96G36	Eclogite	3300	0.23	0.19	0.103	0.069	0.022	0.033	0.006	0.061
BC30	Wehrlite	3300	0.60	0.50	0.013	0.081	0.058	0.004	0.007	0.069
BC200	Clinopyroxenite	3300	0.09	0.07	0.039	0.220	0.009	0.012	0.019	0.040
BC220	Peridotite	3300	0.20	0.17	0.091	0.201	0.019	0.029	0.017	0.066
CP87	Lherzolite	3300	0.93	0.77	0.8	1.4	0.089	0.255	0.122	0.466
CP71	Lherzolite	3300	0.24	0.20	0.3	0	0.023	0.096	0.000	0.119
CP150	Websterite	3300	0.00	0.00	0.2	0.06	0.000	0.064	0.005	0.069
CP28	Websterite	3300	0.00	0.00	0.08	0.16	0.000	0.026	0.014	0.039
CP69	Harzburgite	3300	0.21	0.17	0.3	0.17	0.020	0.096	0.015	0.131
CP96	Websterite	3300	0.00	0.00	0.3	0.56	0.000	0.096	0.049	0.144
CP36	Clinopyroxenite	3300	0.00	0.00	0.3	0.56	0.000	0.096	0.049	0.144
CP161	Clinopyroxenite	3300	0.00	0.00	0.1	0	0.000	0.032	0.000	0.032
CP179	Orthopyroxenite	3300	0.00	0.00	0.07	0.2	0.000	0.022	0.017	0.040
CP166	Clinopyroxenite	3300	0.15	0.12	0.11	0.23	0.014	0.035	0.020	0.069
CP92	Orthopyroxenite	3300	0.03	0.03	0.7	0.08	0.003	0.223	0.007	0.233
CP119	Websterite	3300	0.00	0.00	2.5	0.3	0.000	0.798	0.026	0.824
CP50	Websterite	3300	0.00	0.00	0	0	0.000	0.000	0.000	0.000
									Average:	0.136

All data come from xenoliths entrained in Miocene or older volcanics (Ducea, 2004).
[a] Densities were not measured for each sample, 3300 kg/m3 was chosen as a reasonable value for upper mantle lithologies.

Th (Mukhopadhyay and Manton, 1994; Ducea et al., 2005), which would increase its heat production relative to ancient cratonic regions.

If the mantle wedge from ~40–125 km depth had an average heat production of 0.14 μW/m^3, then it should contribute ~12 mW/m^2 to the surface heat flux. This is slightly greater than the maximum mantle heat flux calculated by subtracting our model crustal heat production from the average surface heat flow. This, in turn, suggests that no heat from deeper portions of the mantle is reaching the surface of the Sierra Nevada, consistent with the idea that a flat, cool Laramide slab was underlying the Sierran lithosphere at ≥125 km. A cool oceanic slab at this depth would refrigerate the overlying lithosphere and insulate it from the deeper portions of the mantle.

6. Conclusions

Radiogenic heat production within the Sierra Nevada batholith is probably not distributed exponentially as a function of depth. Rather, it may be nearly constant at ~2 μW/m^3 through the volcanic pile near the top of the batholith, then increase to values typically near 3–4 μW/m^3 at ~5 km paleodepth, then decreasing again to ~0.5–1 μW/m^3 by ~15 km paleodepth, below which radiogenic heat production may remain more-or-less constant to the base of the crust. The Cretaceous mantle wedge that developed beneath the Sierra Nevada batholith, to depths of ~125 km, appears to have generated heat at a rate of ~0.14 μW/m^3.

The exponential model of HPE distribution has been interpreted as possibly representing the effects of a thin (~10–15 km), highly radiogenic, felsic batholith over an essentially non-radiogenic mid- to lower crust (c.f.Birch et al., 1968; Lachenbruch, 1968, 1970). Our observation of a non-exponential distribution of HPEs and a weak correlation between silica content and HPE abundance refutes such interpretations, and suggests that surface heat flow data provides little constraint on the location or thickness of the felsic batholith.

Our empirically constrained model for the distribution of radiogenic heat production predicts reasonable geothermal gradients that overlap with values determined from thermobarometry. The model also predicts that radiogenic heat production in the Sierran crust accounts for most or all of the present day surface heat flow, implying that the mantle heat flux was very low, at least until ~10 Ma.

The non-exponential form of the depth vs. radiogenic heat production curve proposed herein does not predict or explain a perfectly linear Q_0 vs. A_0 relationship for surface heat flow data. However, given the departures from linearity seen in the Q_0 vs. A_0 plot for the Sierra Nevada (c.f. Fig. 3 of Saltus and Lachenbruch, 1991) this may not be a problem, as the depth vs. radiogenic heat production curve is crudely similar to an exponential at depths below ~5 km and most of the Sierra Nevada has had more than 5 km of material erosionally removed (c.f. Fig. 2). The interpretive model curve may therefore be consistent with the crudely linear Q_0 vs. A_0 data plot.

Acknowledgements

This research was partially supported by NSF grants EAR 00087347 (Ducea and Saleeby), EAR 0230383 (Saleeby), EAR 0087125 and EAR 0229470 (Ducea), and a California State University Bakersfield URC grant (Brady). The authors would like to thank D. Baron, R. Cox, F. Baumeister, and T. Kelly for assistance with analyses and data reduction and J. Ague for providing access to his database of Aluminum in hornblende barometry from the Sierra Nevada batholith. We would also like to thank two anonymous reviewers for their thorough and helpful comments.

References

Ague, J.J., 1997. Thermodynamic calculation of emplacement pressures for batholithic rocks, California: implications for the aluminum-in-hornblende barometer. Geology 25, 563–566.

Ague, J.J., Brimhall, G.H., 1988. Magmatic arc asymmetry and distribution of anomalous plutonic belts in the batholiths of California: effects of assimilation, crustal thickness, and depth of crystallization. Geological Society of America Bulletin 100, 912–927.

Albarede, F., 1975. The heat flow/heat generation relationship: an interaction model of fluids within cooling intrusions. Earth and Planetary Science Letters 27 (73–78).

Ashwal, L.D., Morgan, P., Kelley, S.A., Percival, J.A., 1987. Heat production in an Archean crustal profile and implications for

heat flow and mobilization of heat-producing elements. Earth and Planetary Science Letters 85, 439–450.
Beaumont, C., Jamieson, R.A., Nguyen, M.H., Lee, B., 2001. Himalayan tectonics explained by extrusion of a low-viscosity crustal channel coupled to focused surface denudation. Nature 414, 738–742.
Birch, F., Roy, R.F., Decker, E.R., 1968. Heat flow and thermal history in New England and New York. In: Zen, E., White, W.S., Hadley, J.B., Thompson, J.B.J. (Eds.), Studies of Appalachian Geology: Northern and Maritime. Wiley Interscience, New York, pp. 437–451.
Buntebarth, G., 1976. Distribution of uranium in intrusive bodies due to combined migration and diffusion. Earth and Planetary Science Letters 32, 84–90.
Christensen, N.I., Mooney, W.D., 1995. Seismic velocity structure and composition of the continental crust; a global view. Journal of Geophysical Research, B, Solid Earth and Planets 100 (6), 9761–9788.
Cull, J.P., 1976. The measurement of thermal parameters at high pressures. Pure and Applied Geophysics 114 (2 Selected topics in petrophysics), 301–307.
Dodge, F.C.W., Calk, L.C., Kistler, R.W., 1986. Lower crustal xenoliths, Chinese Peak lava flow, central Sierra Nevada. Journal of Petrology 27, 1277–1304.
Dodge, F.C.W., Lockwood, J.P., Calk, L.C., 1988. Fragments of the mantle and crust from beneath the Sierra Nevada batholith: xenoliths in a volcanic pipe near Big Creek, California. Geological Society of America Bulletin 100, 938–947.
Ducea, M., 2001. The California Arc; thick granitic batholiths, eclogitic residues, lithospheric-scale thrusting, and magmatic flare-ups. GSA Today 11 (11), 4–10.
Ducea, M., 2002. Constraints on the bulk composition and root foundering rates of continental arcs; a California Arc perspective. Journal of Geophysical Research 107 (B11), 2304. doi:10.1029/2001JB000643.
Ducea, M., 2004, Major, trace and isotopic analyses of xenoliths from the Sierra Nevada (published and unpublished). Data from Ducea and Saleeby, Clemens-Knott, and Dodge, http://www.geo.arizona.edu/tectonics/Ducea/databases/data.html.
Ducea, M.N., Saleeby, J.B., 1996. Buoyancy sources for a large, unrooted mountain range, the Sierra Nevada, California; evidence from xenolith thermobarometry. Journal of Geophysical Research 101, 8224–8229.
Ducea, M., Saleeby, J., 1998a. A case for delamination of the deep batholithic crust beneath the Sierra Nevada, California. In: Ernst, W.G., Nelson, C.A. (Eds.), Integrated Earth and Environmental Evolution of the Southwestern United States; the Clarence A. Hall, Jr. volume, pp. 273–288.
Ducea, M., Saleeby, J.B., 1998b. Crustal recycling beneath continental arcs; silica-rich glass inclusions in ultramafic xenoliths from the Sierra Nevada, California. Earth and Planetary Science Letters 156 (1–2), 101–116.
Ducea, M.N., Saleeby, J.B., 1998c. The age and origin of a thick mafic–ultramafic keel from beneath the Sierra Nevada batholith. Contributions to Mineralogy and Petrology 133, 169–185.
Ducea, M.N., Kidder, S., Zandt, G., 2003. Arc composition at mid-crustal depths: insights from the Coast Ridge Belt, Santa Lucia Mountains, California. Geophysical Research Letters 30 (13), 1703. doi:10.1029/2002GL016297.
Ducea, M.N., Saleeby, J., Morrison, J., Valencia, V.A., 2005. Subducted carbonates, metasomatism of mantle wedges, and possible connections to diamond formation: an example from California. American Mineralogist 90, 864–870.
Dumitru, T.A., 1990. Subnormal Cenozoic geothermal gradients in the extinct Sierra Nevada magmatic arc: consequences of Laramide and post-Laramide shallow-angle subduction. Journal of Geophysical Research 95, 4925–4941.
Dumitru, T.A., Gans, P.B., Foster, D.A., Miller, E.L., 1991. Refrigeration of the western Cordilleran lithosphere during Laramide shallow-angle subduction. Geology 19, 1145–1148.
Emsley, J., 1989. The Elements. Clarendon Press, Oxford.
Fiske, R.S., Tobisch, O.T., 1994. Middle Cretaceous ash-flow tuff and caldera-collapse deposit in the Minarets Caldera, east-central Sierra Nevada, California. Geological Society of America Bulletin 106, 582–593.
Fliedner, M.M., Klemperer, S.L., Christensen, N.I., 2000. Three-dimensional seismic model of the Sierra Nevada Arc, California, and its implications for crustal and upper mantle composition. Journal of Geophysical Research, B, Solid Earth and Planets 105 (5), 10899–10921.
Fliedner, M.M., Ruppert, S., Malin, P.E., Park, S.K., Jiracek, G., Phinney, R.A., et al., 1996. Three-dimensional crustal structure of the southern Sierra Nevada from seismic fan profiles and gravity modeling. Geology (Boulder) 24 (4), 367–370.
Fountain, D.M., 1986. Is there a relationship between seismic velocity and heat production for crustal rocks? Earth and Planetary Science Letters 79, 145–150.
Fountain, D.M., Salisbury, M.H., Furlong, K.P., 1987. Heat production and thermal conductivity of rocks from the Pikwitonei–Sachigo continental cross-section, central Manitoba: implications for the thermal structure of Archean crust. Canadian Journal of Earth Sciences 24, 1583–1594.
Gosnold, W.D., 1987. Redistribution of U and Th in shallow plutonic environments. Geophysical Research Letters 14 (3), 291–294.
Hall, C.A., 1991. Geology of the Point Sur-Lopez Point region, Coast Ranges, California: a part of the Southern California allochthon. Geological Society of America Special Paper 266, 1–40.
Hammarstrom, J.M., Zen, E., 1986. Aluminum in hornblende: an empirical igneous geobarometer. American Mineralogist 71, 1297–1313.
Hart, R.J., Nicolaysen, L.O., Gale, N.H., 1981. Radioelement concentrations in a deep profile through Archean basement of the Vredefort structure. Journal of Geophysical Research 86, 10639–10652.
Henyey, T.L., Lee, T.C., 1976. Heat flow in Lake Tahoe, California–Nevada, and the Sierra Nevada-Basin and Range transition. Geological Society of America Bulletin 87, 1179–1187.
Holt, E.A., 1994, Debris-avalanche emplacement of a Mid-Cretaceous caldera-collapse breccia, Minarets Caldera, Sierra Nevada, CA. M.S. Thesis, Stanford University, Stanford, CA, 52 pp.
Jaupart, C., Mareschal, J.C., 1999. The thermal structure and thickness of continental roots. Lithos 48, 93–114.

Jessop, A.M., 1990. Thermal geophysics. Developments in Solid Earth Geophysics. Elsevier, Amsterdam.

Ketcham, R.A., 1996. Distribution of heat-producing elements in the upper and middle crust of southern and western Arizona: evidence from the core complexes. Journal of Geophysical Research 101, 13611–13632.

Kidder, S., Ducea, M., Gehrels, G., Patchett, J., Vervoort, J., 2003. Tectonic and magmatic development of the Salinian Coast Ridge belt, California. Tectonics 22 (5), 1058. doi:10.1029/2002TC001409.

Kidder, S., Ducea, M., Barbeau, D., Gehrels, G., 2004. The Cretaceous Salinian continental arc: overview and new advances. Abstracts with programs. Geological Society of America 36 (7).

Kremenetsky, A.A., Milanovsky, S.Y., Ovchinikov, L.N., 1989. A heat generation model for continental crust based on deep drilling in the Baltic Shield. Tectonophysics 159, 231–246.

Kumar, P.S., Reddy, G.K., 2004. Radioelements and heat production of an exposed Archean crustal cross-section, Dharwar craton, south India. Earth and Planetary Science Letters 224, 309–324.

Lachenbruch, A.H., 1968. Preliminary geothermal model of the Sierra Nevada. Journal of Geophysical Research 73, 6977–6989.

Lachenbruch, A.H., 1970. Crustal temperature and heat production: implications of the linear heat-flow relation. Journal of Geophysical Research 75, 3291–3300.

Lambert, I.B., Heier, K.S., 1967. The vertical distribution of uranium, thorium, and potassium in the continental crust. Geochimica et Cosmochimica Acta 31, 377–390.

Lee, C.T., Yin, Q., Rudnick, R.L., Chesley, J.T., Jacobsen, S.B., 2000. Osmium isotopic evidence for Mesozoic removal of lithospheric mantle beneath the Sierra Nevada, California. Science 289 (5486), 1912–1916.

Lowe, T.K., 1995. Petrogenesis of the Minarets and Merced Peak volcanic–plutonic complexes, Sierra Nevada, California. Ph.D. Thesis, Stanford University, Stanford, CA, 157 pp.

Mukhopadhyay, B., 1989. Petrology and geochemistry of mafic and ultramafic xenoliths from the Sierra Nevada batholith, Part 1. Ph.D. Thesis, University of Texas at Dallas, Dallas, TX, 215 pp.

Mukhopadhyay, B., Manton, W.I., 1994. Upper mantle fragments from beneath the Sierra Nevada batholith—partial fusion, fractional crystallization, and metasomatism in a subduction-related ancient lithosphere. Journal of Petrology 35, 1418–1450.

Nicolaysen, L.O., Hart, R.J., Gale, N.H., 1981. The Vredefort radioelement profile extended to supracrustal strata at Carletonville, with implications for continental heat flow. Journal of Geophysical Research 86 (B11), 10653–10661.

Pickett, D.A., 1991. An isotopic and petrologic study of an exposure of the deep Sierra Nevada batholith, Tehachapi Mountains, California. Ph.D. Thesis, California Institute of Technology, Pasadena, CA, 338 pp.

Pickett, D.A., Saleeby, J.B., 1993. Thermobarometric constraints on the depth of exposure and conditions of plutonism and metamorphism at deep levels of the Sierra Nevada batholith, Tehachapi Mts., California. Journal of Geophysical Research 98, 609–629.

Roy, R.F., Blackwell, D.D., Birch, F., 1968. Heat generation of plutonic rocks and continental heat flow provinces. Earth and Planetary Science Letters 5, 1–12.

Rudnick, R.L., McDonough, W.F., O'Connell, R.J., 1998. Thermal structure, thickness and composition of continental lithosphere. Chemical Geology 145, 395–411.

Ruppert, S., Fliedner, M.M., Zandt, G., 1998. Thin crust and active upper mantle beneath the southern Sierra Nevada in the Western United States. In: Klemperer Simon, L., Mooney Walter, D. (Eds.), Deep Seismic Profiling of the Continents; I. General Results and New Methods. Tectonophysics, pp. 237–252.

Rybach, L., Buntebarth, G., 1984. The variation of heat generation, density, and seismic velocity with rock type in the continental lithosphere. Tectonophysics 103, 335–344.

Rybach, L., Buntebarth, G., 1987. The relationship between seismic velocity and heat production – critical comments. Earth and Planetary Science Letters 83, 175–177.

Saleeby, J.B., 1990. Progress in tectonic and petrogenetic studies in an exposed cross-section of young (approximately 100 Ma) continental crust, southern Sierra Nevada, California. In: Salisbury Matthew, H., Fountain David, M. (Eds.), Exposed Cross-Sections of the Continental Crust; Proceedings. NATO ASI Series. Series C: Mathematical and Physical Sciences. D. Reidel Publishing Company, Dordrecht-Boston, International, pp. 137–158.

Saleeby, J., 2003. Segmentation of the Laramide slab— evidence from the southern Sierra Nevada region. Geological Society of America Bulletin 115 (6), 655–668.

Saleeby, J., Ducea, M., Clemens-Knott, D., 2003. Production and loss of high-density batholithic root—southern Sierra Nevada, California. Tectonics 22, 1064. doi:10.1029/2002TC001374.

Saltus, R.W., Lachenbruch, A.H., 1991. Thermal evolution of the Sierra Nevada: tectonic implications of new heat flow data. Tectonics 10, 325–344.

Savage, M.K., Li, L., Eaton, J.P., Jones, C.H., Brune, J.N., 1994. Earthquake refraction profile of the root of the Sierra Nevada. Tectonics 13, 803–817.

Sawka, W., Chapell, B.W., 1988. Fractionation of uranium, thorium, and rare earth elements in a vertically zoned granodiorite: implications for heat production distributions in the Sierra Nevada batholith, California, U.S.A. Geochimica et Cosmochimica Acta 52, 1131–1143.

Schmidt, M.W., 1992. Amphibole composition as a function of pressure: an experimental calibration of the Al-in-hornblende barometer. Contributions to Mineralogy and Petrology 110, 304–310.

Shapiro, S.S., Hager, B.H., Jordan, T.H., 1999. Stability and dynamics of the continental tectosphere. In: van der Hilst, R.D., McDonough, W.F. (Eds.), Composition, Deep Structure and Evolution Of Continents. Lithos. Elsevier, Amsterdam, International, pp. 115–133.

Swanberg, C.A., 1972. Vertical distribution of heat production in the Idaho batholith. Journal of Geophysical Research 77, 2508–2513.

Swanberg, C.A., Blackwell, D.D., 1973. Areal distribution and geophysical significance of heat generation in the Idaho batholith and adjacent intrusions in eastern Oregon and western Montana. Geological Society of America Bulletin 84, 1261–1282.

Turcotte, D.L., Oxburgh, E.R., 1972. Statistical thermodynamic model for the distribution of crustal heat sources. Science 176 (1021–1022).

Tuttle, O.F., Bowen, N.L., 1958. Origin of granite in the light of experimental studies in the system $NaAlSi_3O_8$–$KAlSi_3O_8$–SiO_2–H_2O. Geological Society of America Memoir 74, 153.

Wernicke, B., Clayton, R., Ducea, M., Jones, C.H., Park, S., Ruppert, S., et al., 1996. Origin of high mountains in the continents: the southern Sierra Nevada. Science 271, 190–193.

Zandt, G., 2003. The southern Sierra Nevada drip and the mantle wind direction beneath the southwestern United States. In: Klemperer Simon, L., Ernst, W.G. (Eds.), The Lithosphere of Western North America and its Geophysical Characterization.